

# Two-stage Design for Failure Probability Estimation with Gaussian Process Surrogates

Annie S. Booth\*      S. Ashwin Renganathan†

July 8, 2025

## Abstract

We tackle the problem of quantifying failure probabilities for expensive deterministic computer experiments with stochastic inputs under a fixed budget. The computational cost of the computer simulation prohibits direct Monte Carlo (MC) and necessitates a surrogate model, which may facilitate either a “surrogate MC” estimator or a surrogate-informed importance sampling estimator. We embrace the former, finding importance sampling too variable when budgets are limited, and propose a novel design strategy to effectively train a surrogate for the purpose of failure probability estimation. Existing works exhaust the entire evaluation budget on active learning through sequential contour location (CL), attempting to balance exploration with exploitation of the failure contour throughout the design, but we find exhaustive CL to be suboptimal. Instead we propose a novel two-stage surrogate design. In Stage 1, we conduct sequential CL to locate the failure contour. In Stage 2, once surrogate learning has saturated, we use a solely exploitative strategy – allocating the remaining evaluation budget to MC samples with the highest classification entropy to ensure they are classified correctly. We propose a stopping criterion to determine the transition between stages without any tuning. Our two-stage design outperforms alternatives, including exhaustive CL and surrogate-informed importance sampling, on a variety of benchmark exercises. With these tools, we are able to effectively estimate small failure probabilities with only hundreds of simulator evaluations, showcasing functionality with both shallow and deep Gaussian process surrogates, and deploying our method on a simulation of fluid flow around an airfoil.

**Keywords:** active learning, contour location, deep Gaussian process, entropy, importance sampling

## 1 Introduction

Quantifying the probability of failure in complex systems is of great interest but is challenging due to the computational expense of the so-called “computer experiment.” Consider a deterministic black-box computer simulation,  $f : \mathcal{X} \rightarrow \mathbb{R}$  with inputs  $\mathcal{X} \subset \mathbb{R}^d$  governed by known measure  $\mathbb{P}_{\mathbf{x}}$  (with density  $p(\mathbf{x})$ ). The response is thresholded such that  $f(\mathbf{x}) > t$  indicates failure. The research objective is to estimate the failure probability,

$$\alpha = \int \mathbb{1}_{\{f(\mathbf{x}) > t\}} d\mathbb{P}_{\mathbf{x}} = \int_{\mathbf{x} \in \mathcal{X}} \mathbb{1}_{\{f(\mathbf{x}) > t\}} p(\mathbf{x}) d\mathbf{x}, \quad (1)$$

from a small, fixed budget of simulator evaluations.

---

\*Corresponding author: Department of Statistics, Virginia Tech, [annie\\_booth@vt.edu](mailto:annie_booth@vt.edu)

†Department of Aerospace Engineering, Penn State

We are particularly motivated by aeronautic applications where system failures may incur immense financial or environmental costs, or even loss of life. In aircraft design and development, computer simulation experiments are a natural, often mandatory, precursor to direct experimentation and prototyping. For example,  $f(\cdot)$  may represent the vibrations experienced by an aircraft which become unsafe above certain levels, or the fuel efficiency of an aircraft, which if too low, can be detrimental to the environment, obliterate fuel budgets, or overly restrict travel distances. Inputs  $\mathcal{X}$  may encapsulate design parameters and operating conditions (such as wing shapes, flight speeds, and angles of attack). Yet we acknowledge a slew of other relevant applications where quantifying failure probabilities for complex simulations is critical, including structural reliability analysis using finite element simulations (e.g., [Mia et al., 2017](#)), Boltzmann modeling of chemical processes in fuel filtration (e.g., [Belot et al., 2021](#)), and thermodynamic flows for nuclear reactors (e.g., [Batet et al., 2014](#)).

A rudimentary approach to solve Eq. (1) involves brute force Monte Carlo (MC): sample a large number of inputs, evaluate the computer simulation at each of these configurations, and report the proportion that resulted in failure. But this approach is prohibitively expensive if the computer simulation is costly and  $\alpha$  is small, as in our target application. In the face of expensive data, statistical models ( $\hat{f}$ , called “surrogates” or “emulators”) are essential. Surrogates are trained on a limited set of simulator evaluations in order to provide predictions with appropriate uncertainty quantification (UQ) at unobserved inputs. Gaussian processes (GPs) are the canonical choice ([Santner et al., 2018](#); [Gramacy, 2020](#)), but deep Gaussian processes (DGPs; [Damianou and Lawrence, 2013](#)) are becoming increasingly popular, particularly for nonstationary computer experiments ([Booth et al., 2024a](#)). Notably, our contribution is agnostic to surrogate choice as long as effective UQ is provided, and is thus applicable to traditional GPs and Bayesian DGPs ([Sauer et al., 2023b](#)) and, potentially, Bayesian neural networks ([MacKay, 1995](#)).

We briefly digress to acknowledge some early methods of failure probability estimation, namely the first and second order reliability methods (FORM/SORM; [Haldar and Mahadevan, 1995](#)), which leveraged simplistic linear approximations of the complex model and placed all failure probability estimation in the hands of the “most probable point” (MPP). Although advancements to FORM and SORM have been made with more flexible GP models (e.g., [Zhang et al., 2015](#); [Su et al., 2017](#)), sole reliance on a MPP is too restricting for our target applications.

The utility of a surrogate boils down to two things: how it is trained and how it is used. To solve Eq. (1), surrogate accuracy in classifying failures is of primary importance. Not all training designs are created equally. Space-filling designs ([Joseph, 2016](#)) may miss failure regions altogether, particularly when training budgets are limited. Instead, it is common to train a surrogate on a small initial design then pair it with a relevant acquisition function to select subsequent inputs for evaluation through the simulator – a process called “active learning” (AL). The goal is to maximize learning from limited evaluations of the expensive simulator. Contour location (CL) is an AL variant which targets learning of a failure contour  $\{\mathbf{x} \in \mathcal{X} \mid f(\mathbf{x}) = t\}$ . CL acquisition functions seek to balance exploitation and exploration by leveraging both predicted distance from the contour and posterior uncertainty. Popular variations fall under expected improvement frameworks ([Bichon et al., 2008](#); [Ranjan et al., 2008](#)), stepwise uncertainty reduction frameworks ([Bect et al., 2012](#); [Chevalier et al., 2014](#); [Azzimonti et al., 2021](#)), or both ([Duhamel et al., 2023](#)). Others utilize pass/fail classification entropy ([Marques et al., 2018](#); [Cole et al., 2023](#)). [Booth et al. \(2024c\)](#) recently proposed a CL sequential design for DGP surrogates. For small failure regions, contour location may be replaced with subset simulation ([Au and Beck, 2001](#)) which initially targets a conservative threshold ( $t^* < t$ ) and iteratively refines it until the true threshold is found ( $t^* \rightarrow t$ ) ([Dubourg et al., 2011](#); [Huang et al., 2016](#); [Hristov et al., 2019](#)). Yet these approaches require Markov chain Monte Carlo (MCMC) sampling of cascading input distributions, which we intentionally avoid here.

A well-trained surrogate may be leveraged directly within an MC estimator with surrogate predictions

(which are of negligible cost) in place of true simulator evaluations, which we term “surrogate MC.” One could reasonably use the entire budget of simulator evaluations for contour location, then deploy the trained surrogate in such a “surrogate MC” estimator. Although this is common (e.g., [Zhu and Du, 2016](#); [Cheng and Lu, 2020](#); [Li et al., 2021](#); [Lu et al., 2023](#)), we find that surrogate learning of failure contours quickly plateaus, and that common surrogates fail to achieve sufficient classification accuracy under tightly restricted evaluation budgets.

Another common approach splits the budget of simulator evaluations into two disjoint stages: some evaluations are used to train a surrogate and some are used for importance sampling (IS; [Srinivasan, 2002](#); [Tokdar and Kass, 2010](#)). IS hinges on the construction of a bias distribution that intentionally focuses density in the failure region. Inputs are sampled from the bias distribution and are then utilized in a weighted average calculation that corrects for the disparity between the bias density and the original input density. Identifying an effective bias distribution in the face of limited training data is a hefty task ([Tabandeh et al., 2022](#)). Adaptive methods abound (e.g., [Oh and Berger, 1992](#); [Kurtz and Song, 2013](#); [Dalbey and Swiler, 2014](#); [Bugallo et al., 2017](#); [Cheng et al., 2023](#)). [Peherstorfer et al. \(2016\)](#) propose what they termed “multifidelity importance sampling,” although we prefer the term “surrogate-informed importance sampling” (SIIS) to avoid confusion with multifidelity surrogate modeling (e.g., [Park et al., 2017](#)). In SIIS, a trained surrogate is used to identify predicted failures, and a bias distribution is fit to these locations (more on this in Section 2.3). SIIS has been deployed with GP surrogates in a variety of subsequent works (e.g., [Cole et al., 2023](#); [Renganathan et al., 2023](#); [Booth et al., 2024b](#); [Renganathan, 2024](#)), and we view it as our primary competitor. Yet SIIS has several crucial drawbacks. We will delay a thorough discussion to Section 2.3, but the highlights are: (i) SIIS relies too heavily on an arbitrary bias distribution, (ii) it largely ignores the carefully trained surrogate, and (iii) it offers no guidance for allocating the budget between surrogate training and IS estimation.

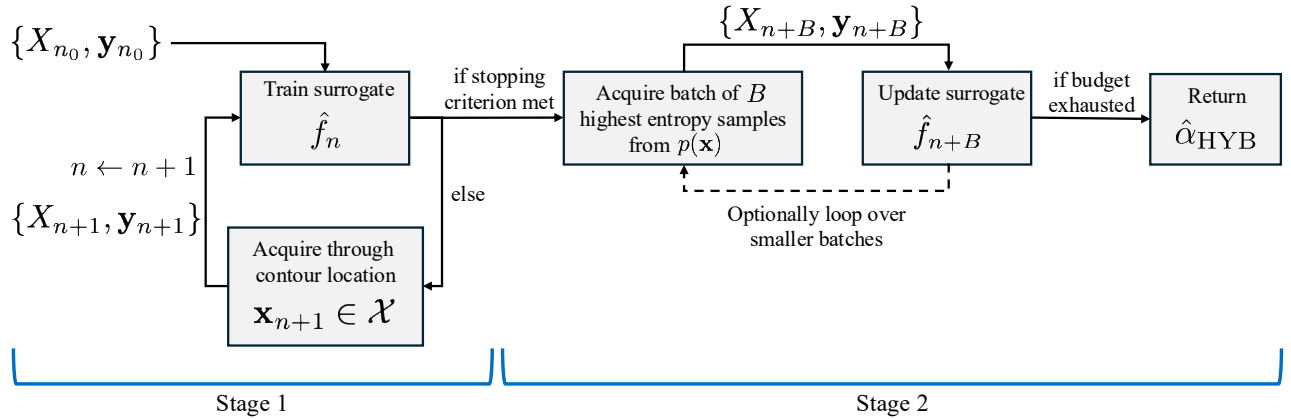


Figure 1: Overview of proposed two-stage design for failure probability estimation. Stage 1 uses contour location to balance exploitation and exploration of  $\{\mathbf{x} \in \mathcal{X} \mid f(\mathbf{x}) = t\}$ . Stage 2 solely exploits high uncertainty Monte Carlo samples from  $p(\mathbf{x})$ . For a fixed budget of  $n + B$ , our approach determines how to effectively allocate  $n$  (for contour location) and  $B$  (for Monte Carlo estimation).

We prefer to avoid a bias distribution altogether, instead focusing on how we could optimally leverage a surrogate and an MC estimator in tandem. The answer lies in a two-stage surrogate design, represented in Figure 1 with details reserved for Section 3. First, in Stage 1 we conduct traditional contour location, balancing exploration and exploitation while locating the failure contour within domain  $\mathcal{X}$ . As training progresses, successive acquisitions will offer less additional insight, indicated by apparent convergence

of the “surrogate MC” estimator. Although we can not be sure of theoretical convergence with our limited budget, we propose a stopping criterion to recognize practical convergence (when surrogate learning from CL has saturated). Once this stopping criterion is met, instead of continuing contour location or turning to importance sampling, we propose a novel “Stage 2” in which the remaining simulation budget is spent precisely on the *Monte Carlo samples from  $p(\mathbf{x})$  with the highest classification entropy*. By observing the true  $f(\mathbf{x})$  for samples where our surrogate is uncertain, we ensure these locations are classified correctly within our final MC estimate. Ultimately, surrogates trained on the observations acquired in these two unique stages provide more accurate and precise MC estimates of  $\alpha$ . While we prefer to view our contribution through the lens of surrogate design, our final failure probability estimate may be considered a “hybrid MC” estimator which combines the true simulator observations from Stage 2 with surrogate predictions at unobserved samples.

This manuscript is laid out as follows. Section 2, reviews GP/DGP surrogates, contour location, and importance sampling. Section 3 presents our two-stage design and failure probability estimator. Section 4 presents a variety of synthetic benchmarks. Finally, we deploy our method on a computer experiment of an RAE-2822 airfoil in Section 5 and conclude in Section 6.

## 2 Preliminaries

Denote single inputs as the row vector  $\mathbf{x}$  of size  $1 \times d$  with response  $y = f(\mathbf{x})$ , where  $f$  represents the black-box computer simulation. Let  $X_n$  represent the row-combined matrix of  $n$ -many inputs with corresponding response vector  $\mathbf{y}_n$ . Our objective is to quantify the failure probability from Eq. (1), namely  $P(f(\mathbf{x}) > t)$  for  $\mathbf{x} \sim p(\mathbf{x})$ . Brute force Monte Carlo with a budget of size  $M$  provides the estimator

$$\hat{\alpha}_{\text{MC}} = \frac{1}{M} \sum_{i=1}^M \mathbb{1}_{\{f(\mathbf{x}_i) > t\}} \quad \text{for } \mathbf{x}_i \stackrel{\text{iid}}{\sim} p(\mathbf{x}), \quad (2)$$

but this estimator is infeasible when  $f$  is expensive. Let  $N$  denote the total budget of expensive simulator evaluations allotted. We will describe our sample efficient method for estimating failure probabilities in Section 3, targeting  $N$  in the hundreds, after a quick review of preliminaries.

### 2.1 Gaussian process surrogates

A surrogate model  $\hat{f}$ , trained on a limited budget of simulations, may provide predictions for unobserved inputs in place of the true  $f$ . To enable our proposed methodology, the surrogate must also provide uncertainty quantification through posterior predictive distributions. Gaussian processes (GPs) are the predominant choice; they assume a multivariate normal distribution over the response. For any  $n$  observed locations, our GP prior assumption is  $\mathbf{y}_n \sim \mathcal{N}_n(\boldsymbol{\mu}, \Sigma(X_n))$ . The prior mean  $\boldsymbol{\mu}$  is often simplified to the zero vector after centering (which we will use moving forward), and the prior covariance  $\Sigma(X_n)$  is typically a function of Euclidean distances, e.g.,  $\Sigma(X_n)^{ij} = \Sigma(\mathbf{x}_i, \mathbf{x}_j) = k(\|\mathbf{x}_i - \mathbf{x}_j\|^2)$  with kernel  $k(\cdot)$ . See [Santner et al. \(2018\)](#); [Rasmussen et al. \(2006\)](#); [Gramacy \(2020\)](#) for thorough reviews. Conditioned on training data  $\{X_n, \mathbf{y}_n\}$ , posterior predictions at singleton input  $\mathbf{x}$  follow

$$\hat{f}_n(\mathbf{x}) \sim \mathcal{N}_1(\mu_n(\mathbf{x}), \sigma_n^2(\mathbf{x})) \quad \text{for} \quad \begin{aligned} \mu_n(\mathbf{x}) &= \Sigma(\mathbf{x}, X_n) \Sigma(X_n)^{-1} \mathbf{y}_n \\ \sigma_n^2(\mathbf{x}) &= \Sigma(\mathbf{x}, \mathbf{x}) - \Sigma(\mathbf{x}, X_n) \Sigma(X_n)^{-1} \Sigma(\mathbf{x}, X_n)^\top \end{aligned} \quad (3)$$

where  $\Sigma(\mathbf{x}, X_n)$  denotes the vector formed from applying the kernel between  $\mathbf{x}$  and every row of  $X_n$ . Joint predictions are straightforward but not necessary for our contribution.

A natural alternative to brute force MC (2) is “surrogate MC” which leverages surrogate predictions in place of the true simulator,

$$\hat{\alpha}_{\text{SURR}} = \frac{1}{M} \sum_{i=1}^M \mathbb{1}_{\{\mu_n(\mathbf{x}_i) > t\}} \quad \text{for } \mathbf{x}_i \stackrel{\text{iid}}{\sim} p(\mathbf{x}). \quad (4)$$

Here we use the posterior mean of our surrogate  $\hat{f}$  in place of the true  $f$ . This estimator, however, inherits the bias of the surrogate – if the surrogate is not accurate near the contour, it will misclassify inputs which will severely hinder the effectiveness of this estimator.

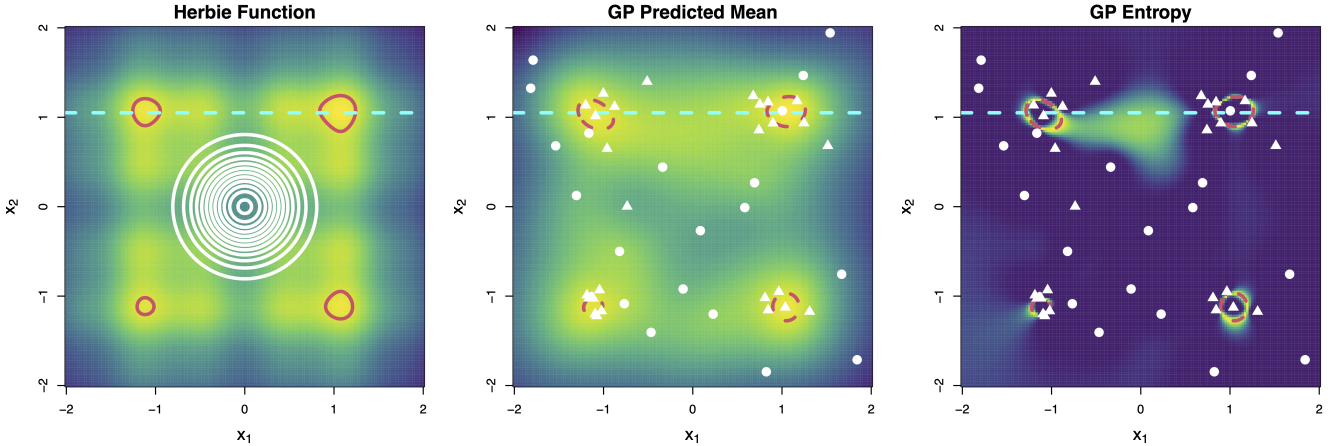


Figure 2: *Left:* Herbie function (yellow/high, purple/low) with true failure contour (red) and input distribution (white). *Center/Right:* Posterior predicted mean and entropy of a GP trained on an initial 20-point LHS (white circles) followed by 30 contour locating acquisitions (white triangles). Predicted contour in dashed red. Dashed line at  $x_2 = 1.05$  indicates the slice shown in Figure 3.

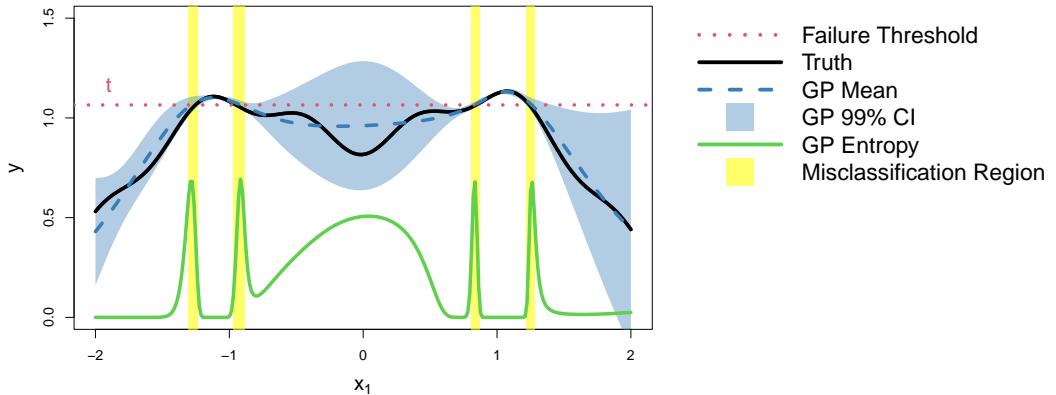


Figure 3: Slice of Herbie function along  $x_2 = 1.05$  (solid black) with failure threshold (dotted red). GP surrogate from Figure 2 shown in blue, with entropy in green along the  $x$ -axis. Yellow shaded regions indicate inputs which the surrogate would misclassify.

For example, consider the two-dimensional “Herbie” function (Lee et al., 2011) shown in the left panel of Figure 2 (we will revisit the other panels momentarily). We define a failure threshold of  $t = 1.065$  which

demarcates four disjoint failure regions (red contours). We also define  $p(\mathbf{x})$  using independent normal distributions centered at the origin (white contours).<sup>1</sup> We trained a GP surrogate using an initial random Latin hypercube sample (LHS; [McKay et al., 2000](#)) of size  $n_0 = 20$  (white circles), followed by 30 contour locating acquisitions (white triangles, discussed in Section 2.2). Figure 3 shows the GP posterior along the slice  $x_2 = 1.05$ . The posterior mean (dashed blue) and 99% credible interval (blue shading) capture the true nonlinear surface (solid black) fairly well. Even so, there are inputs (highlighted by the yellow shading) which the surrogate would misclassify as “passes” instead of “failures” or vice versa. While the predictions in these regions are reasonably accurate, their proximity to the contour makes precise classification difficult.

**Deep Gaussian processes.** In some situations, surrogate predictions may be improved through adaptations to the surrogate model itself. Traditional GPs are limited by the commonly assumed stationarity of the covariance kernel; they are not able to accurately model nonstationary surfaces characterized by regime shifts and stark transitions. Deep Gaussian processes ([Damianou and Lawrence, 2013](#)) are a promising more flexible alternative. They leverage functional compositions of GP layers in which latent layers act as warped versions of the original inputs, allowing for greater flexibility. DGPs have consistently outperformed stationary GPs in modeling nonstationary computer experiments (e.g., [Rajaram et al., 2021](#); [Yazdi, 2022](#); [Ming et al., 2023](#)), particularly when deployed in a Bayesian framework using MCMC sampling to achieve full posterior integration of latent layers (e.g., [Sauer et al., 2023b,a](#)). See [Sauer \(2023\)](#) for a thorough review of DGP surrogates. Crucially, our method is agnostic to surrogate choice as long as UQ is provided. We will demonstrate functionality with both traditional GP and Bayesian DGP surrogates in Section 4.

## 2.2 Contour location

To facilitate failure probability estimation (4), a surrogate must accurately classify passes and failures. Strategic sequential designs targeting the failure contour, i.e., “contour location,” will outperform space-filling counterparts in this regard. In CL, after initializing with a small space-filling design, subsequent training locations are selected iteratively through the optimization of an acquisition criterion. The computer simulation is evaluated at the selected input(s), the surrogate is updated, and the process is repeated until the budget is exhausted or a stopping criterion is met. Stage 1 of Figure 1 visualizes this iterative loop. While acquisitions may be made in batches, we only consider single acquisitions here.

Identifying acquisition criteria which effectively target failure contours is a hot topic, particularly in conjunction with GP surrogates, (e.g., [Bichon et al., 2008](#); [Ranjan et al., 2008](#); [Bect et al., 2012](#); [Chevalier et al., 2014](#); [Marques et al., 2018](#); [Cole et al., 2023](#)). Here, we highlight one in particular – classification entropy – defined as

$$H(\mathbf{x}) = -p_{\mathbf{x}} \log(p_{\mathbf{x}}) - (1 - p_{\mathbf{x}}) \log(1 - p_{\mathbf{x}}), \quad (5)$$

where  $p_{\mathbf{x}}$  represents the predicted probability of failure at input  $\mathbf{x}$ , i.e.,  $P(\hat{f}_n(\mathbf{x}) > t)$ . With a GP surrogate, this predicted probability boils down to a Gaussian CDF computation,

$$p_{\mathbf{x}} = P\left(\hat{f}_n(\mathbf{x}) > t\right) = 1 - \Phi\left(\frac{t - \mu_n(\mathbf{x})}{\sigma_n(\mathbf{x})}\right),$$

with  $\mu_n(\mathbf{x})$  and  $\sigma_n(\mathbf{x})$  following Eq. (3). Revisiting the Herbie example of Section 2.1, we offer two visuals of the entropy surface for the trained GP. First, the right panel of Figure 2 shows entropy over the entire 2d space. Notice high entropy regions are predominantly near the failure contour and/or away from training data locations. Second, Figure 3 shows the entropy surface (green) along the slice  $x_2 = 1.05$ . Entropy is

---

<sup>1</sup>Full details of all simulated functions, thresholds, and distributions are provided in the Supplementary Material.

high where the credible interval (blue shading) captures the failure threshold (dotted red). It is influenced by how much of the credible interval is split above/below  $t$ , regardless of the interval's width. For the highest  $x_1$  values, surrogate uncertainty is high but entropy is low because the predicted values are far from the failure threshold. As an acquisition criterion, entropy effectively identifies regions where the surrogate is uncertain of its pass/fail prediction. A reasonable acquisition could fall in any of the local optima of the entropy surface.

Naturally, implementations of entropy as an acquisition function vary on the finer details. For GP surrogates we will leverage the optimization scheme of Cole et al. (2023), which first deploys a small LHS, identifies the LHS sample with the highest entropy, then runs a numerical optimization of entropy initialized at that point. By avoiding multi-starts, Cole et al. target local optima in the entropy surface. For DGP surrogates, we will follow Booth et al. (2024c). To avoid cumbersome numerical optimizations with the heftier MCMC-based DGP, Booth et al. use triangulation candidates (Gramacy et al., 2022), then select the candidate on the Pareto front of entropy and uncertainty. Henceforth, all GPs and DGPs we consider will be trained with these two contour location methods, respectively.

The right and center panels of Figure 2 showed a contour locating design for the Herbie function. Starting with a GP surrogate trained on an LHS design of size  $n_0 = 20$  (white circles), we used the entropy-based scheme of Cole et al. (2023) to acquire 30 more inputs, one-at-a-time (white triangles). The acquired points attempt to balance exploring the space and exploiting learning of the failure contour.

### 2.3 Importance sampling

Rather than side-stepping the prohibitive computation of Eq. (1) with surrogate evaluations, importance sampling (Tokdar and Kass, 2010) avoids expensive evaluations by sampling from a different distribution altogether. Let  $q(\mathbf{x})$  denote a “bias” density which shares domain with  $p(\mathbf{x})$ . The failure probability  $\alpha$  may be equivalently represented as

$$\alpha = \int_{\mathbf{x} \in \mathcal{X}} \mathbb{1}_{\{f(\mathbf{x}) > t\}} \frac{p(\mathbf{x})}{q(\mathbf{x})} q(\mathbf{x}) d\mathbf{x}.$$

Monte Carlo approximation of this integral provides the estimator,

$$\hat{\alpha}_{\text{IS}} = \frac{1}{B} \sum_{i=1}^B w_i \mathbb{1}_{\{f(\mathbf{x}_i) > t\}} \quad \text{where} \quad w_i = \frac{p(\mathbf{x}_i)}{q(\mathbf{x}_i)} \quad \text{for} \quad \mathbf{x}_i \stackrel{\text{iid}}{\sim} q(\mathbf{x}). \quad (6)$$

This estimator requires  $B$ -many evaluations of the expensive simulator  $f$ . The “bias weights”  $w_i$  account for the difference between the input density and the bias density. This estimator is theoretically unbiased for any  $B > 0$  and requires a smaller budget of simulator evaluations ( $B \ll M$ ) if the bias distribution appropriately covers and targets the failure region (Srinivasan, 2002). But estimation of an effective bias distribution is tricky. The ideal bias distribution is  $q(\mathbf{x})^* = \frac{1}{\alpha} \mathbb{1}_{\{f(\mathbf{x}) > t\}} p(\mathbf{x})$ , but neither  $\alpha$  nor the indicator function are known *a priori*. For the sake of feasibility,  $q(\mathbf{x})$  is traditionally constrained to a known distributional family, such as a Gaussian mixture model (GMM; Reynolds et al., 2009). Bias distribution training is then relegated to learning distributional parameters (in a GMM, these include the number of mixtures, mixture weights, and component means and variances), often accomplished through cross validation or information criteria maximization.

In “surrogate-informed importance sampling,” Peherstorfer et al. (2016) leverage a surrogate to identify predicted failures from a large Monte Carlo sample of the input distribution, then train a GMM bias distribution to these predicted failures. Recent works have leveraged contour location to train surrogates for this very purpose (e.g., Cole et al., 2023; Booth et al., 2024b). If the surrogate effectively identifies the

failure region, then these samples should mimic the ideal  $q(\mathbf{x})^*$ . With a trained bias distribution in-hand, samples may be drawn from  $q(\mathbf{x})$ , evaluated through the expensive simulator, and deployed in Eq. (6) to provide an estimate of the failure probability. SIIS is a two-stage enterprise (first training a surrogate then using the surrogate to estimate a bias distribution for importance sampling), but it is not a “two-stage design” since the final estimator makes no use of the surrogate nor the observations that had been used to train the surrogate.

Although SIIS has been widely embraced for its unbiasedness, it has several key weaknesses. First, the bias distribution, which features heavily in the final estimate of Eq. (6), is a completely auxiliary quantity. Hypothetically, two different bias distributions could produce the same samples  $\{\mathbf{x}_i\}_{i=1}^B$ , thus producing the same  $\{f(\mathbf{x}_i)\}_{i=1}^B$ . But in the calculation of Eq. (6), these two bias distributions would contribute different weights, resulting in different final answers even though the training data from the computer simulator was exactly the same. O’Hagan (1987) first pointed out this conundrum as a violation of the “Likelihood principle.” A second weakness is the restriction of  $q(\mathbf{x})$  to distributional families like GMMs. Failure regions may be complex and may not fit nicely under these target distributions. Consequently, SIIS typically requires large  $B$  in order to adequately cover the failure region. For context, Peherstorfer et al. (2016) entertained  $B \in \{100, 1000, 10000, 100000\}$  and found performance continued to improve as  $B$  increased. Furthermore, there is no clear avenue for determining the budget allocation between surrogate training and importance sampling estimation. [In our benchmark exercises, we will borrow from our proposed method to inform budget allocation for the SIIS competitor.] Finally, the SIIS method does not leverage the full potential of the surrogate model. Many expensive simulator evaluations go into training the surrogate, but the surrogate is abandoned after it has identified potential bias locations for estimation of  $q(\mathbf{x})$ .

### 3 Two-stage design for failure probability estimation

Ultimately, we are unsatisfied with the two aforementioned surrogate-based methods for estimating  $\alpha$ : exhaustive CL with surrogate MC and surrogate-informed importance sampling. While the drawbacks to SIIS are apparent, the limitations of exhaustive CL deserve more attention. To investigate further, we revisit the CL design of the Herbie function (Figure 2), this time continuing contour location until an entire budget of  $N = 150$  has been exhausted. As the design progresses, we evaluate and store the surrogate MC estimate  $\hat{\alpha}_{\text{SURR}}$  (4), which we now denote as simply  $\hat{\alpha}$ , after every 10th CL acquisition. Progress in this estimate is shown in the left panel of Figure 4. While there is significant learning occurring with early acquisitions, it quickly plateaus. By the time the surrogate has been trained on 100 points, it knows just as much about  $\alpha$  as it does when it has been trained on the full budget of  $N = 150$  points. In this case, continued contour location is effectively wasting the remaining simulation budget. We propose a solution: first developing a stopping criterion to decide when to halt contour location (Figure 1, Stage 1), then proposing a second design stage (Figure 1, Stage 2) which greedily leverages the remaining simulation budget for Monte Carlo samples with the highest classification uncertainty. The second stage, in which observations are acquired directly from  $p(\mathbf{x})$  enables a “hybrid Monte Carlo” estimator, using both true simulator observations and surrogate predictions.

#### 3.1 A stopping criterion for contour location

Let  $n$  denote the budget of expensive simulator evaluations used on contour location (Stage 1). Let  $B$  denote the remaining evaluation budget, such that the total budget is  $N = n + B$ . We seek an objective, automatable decision rule for selecting  $n$ , halting CL once surrogate learning has plateaued. Consider the

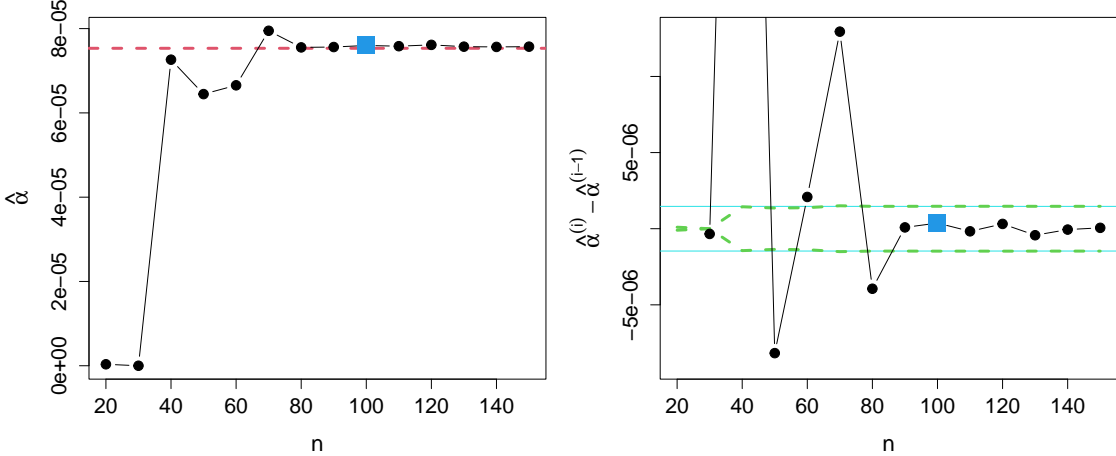


Figure 4: *Left:* Failure probability estimate (4) from a GP surrogate of the Herbie function (as shown in Figure 2), updated after every 10th acquisition of the CL design. True  $\alpha$  in dashed red. *Right:* Difference in successive  $\hat{\alpha}$  estimates with  $\pm\hat{\sigma}_\alpha$  shown in dashed green. Narrow teal line indicates true  $\sigma_\alpha$ . Blue square marks the second update within  $\pm\hat{\sigma}_\alpha$ , which satisfies our proposed stopping criterion.

progress in  $\hat{\alpha}$  shown in Figure 4. The right panel shows the relative difference between each successive  $\hat{\alpha}$  estimate from the left panel. As expected, the relative differences converge to zero as the surrogate hones in on the true contour, but with this finite budget they never settle at exactly zero. We need an objective method to decide when these updates to  $\hat{\alpha}$  are no longer significant.

The challenge is that  $\hat{\alpha}$  exhibits variability from two distinct sources: surrogate error and the natural variability that accompanies any Monte Carlo estimator with finite  $M$ . Hypothetically, presume we could evaluate the true  $f$  an unlimited number of times to obtain the brute force MC estimator of Eq. (2). In this estimator, the indicator  $\mathbb{1}_{\{f(\mathbf{x}) > t\}}$  is a Bernoulli random variable with expected value  $\alpha$  and variance  $\alpha(1 - \alpha)$ . Thus, the MC estimator has variance inversely proportional to  $M$ :

$$\mathbb{V}[\hat{\alpha}_{\text{MC}}] = \frac{1}{M^2} \sum_{i=1}^M \mathbb{V}[\mathbb{1}_{\{f(\mathbf{x}) > t\}}] = \frac{\alpha(1 - \alpha)}{M}.$$

Let  $\sigma_\alpha = \sqrt{\frac{\alpha(1 - \alpha)}{M}}$  denote the standard error of this estimator; it quantifies the degree of variability that we would expect even if we used the true  $f$  (i.e., zero surrogate error). We consider successive updates to  $\hat{\alpha}$  within this realm of intrinsic MC variability to indicate stabilization of the surrogate. Since the true  $\alpha$  is unknown, we estimate  $\hat{\sigma}_\alpha = \sqrt{\frac{\hat{\alpha}(1 - \hat{\alpha})}{M}}$  using the current surrogate MC estimate. While this does intertwine surrogate error and MC error, it still provides a useful and feasible estimate.

To demonstrate, the green dashed lines in the right panel of Figure 4 show  $\pm\hat{\sigma}_\alpha$ , updated with  $\hat{\alpha}$  after every 10th acquisition. The estimated  $\hat{\sigma}_\alpha$  (dashed green) effectively reflects the true  $\sigma_\alpha$  (narrow solid teal) after very few acquisitions. At the start of the design, updates to  $\hat{\alpha}$  are far beyond this estimated standard error. But after a while, the updates sit comfortably within these bounds.

Let  $X_M$  denote the row-combined matrix of  $M$ -many samples from  $p(\mathbf{x})$ . We posit that, for fixed  $X_M$ , any update to  $\hat{\alpha}$  within  $\pm\hat{\sigma}_\alpha$  is insignificant, as it is within the realm of expected MC error. [To avoid excessive computation, we recommend updating estimates after every 10 acquisitions, which we will do in all later exercises.] Accordingly, we propose halting CL once we have observed two successive updates

within  $\pm \hat{\sigma}$ . The blue square in Figure 4 marks this point, stopping CL for this example at  $n = 100$ , effectively identifying a point where surrogate learning has saturated and leaving a remaining budget of  $B = 50$ . Note, this stopping criterion requires the same  $X_M$  be used in every  $\hat{\alpha}$  calculation. If a new  $X_M$  is generated for each estimate, there would be additional sampling variability reflected among the  $\hat{\alpha}$ 's (on top of the surrogate error and MC variability).

Our budgeting scheme is summarized as follows. Initialize a surrogate, begin a contour locating sequential design, and collect one sample  $X_M$ . At the start, it is likely that there will be no failures observed and that  $\hat{\alpha}$  will be equal to zero (as seen in Figure 4). To safeguard against halting surrogate training prematurely, we build in a “common sense” check by setting a minimum number of failures that must be observed before contour location could be halted. If the contour locating design is succeeding, it will be placing some points in the failure region. We recommend a default of 10 failures, but suggest increasing this for more complex, higher dimensional problems. Once the design has surpassed these minimum requirements, estimate  $\hat{\alpha}$  after every 10th acquisition. Calculate  $\hat{\sigma}_\alpha$  and check if  $|\hat{\alpha}^{(\text{current})} - \hat{\alpha}^{(\text{previous})}| < \hat{\sigma}_\alpha$ . When this condition has been satisfied twice in a row, halt the CL design of Stage 1 and proceed to Stage 2 (the topic of Section 3.2).

**Choosing  $M$ .** In practice, it is important to select a MC sample size that is large enough without being too cumbersome. Larger  $M$  will produce more effective sum approximations of the true integrals, but we need surrogate predictions (e.g., Eq. 3) for every sample in  $X_M$ . Although this computation is significantly cheaper than evaluation of the expensive simulator, it could be significant for extremely large  $M$ , particularly with a heftier surrogate like a Bayesian DGP.

If we knew  $\alpha$ , we could determine  $M$  by thresholding the standard error  $\sigma_\alpha$ . For example, to achieve a standard error less than 10% of  $\alpha$  requires:

$$\sigma_\alpha < \frac{\alpha}{10} \quad \rightarrow \quad \frac{100(1 - \alpha)}{\alpha} < M.$$

To achieve this precision,  $\alpha = 10^{-4}$  requires  $M$  nearly 1 million,  $\alpha = 10^{-5}$  requires  $M$  nearly 10 million, and  $\alpha = 10^{-6}$  requires  $M$  nearly 100 million. In practice, with unknown  $\alpha$ , we recommend either choosing  $M$  conservatively given expert insight into the anticipated failure probability or performing a pilot study where  $M$  is incremented say by one million at a time. Gather surrogate predictions along this incremental process, and use  $\hat{\alpha}$  to inform  $\hat{\sigma}_\alpha$ .

### 3.2 Stage 2: Hybrid Monte Carlo for failure probability estimation

Once  $n$  is determined and the contour location of Stage 1 is complete, how should we spend the remaining budget of simulator evaluations ( $B = N - n$ ) in Stage 2? Recall, our objective is to leverage the trained surrogate to estimate  $\alpha$  (1). We propose a new design for Stage 2, which enables an upgrade to the surrogate MC estimator of Eq. (4).

To set the stage, let  $\mathcal{U} \subset \mathcal{X}$  represent some subset of the input domain (boundary inclusive). Then, Eq. (1) may be partitioned as

$$\alpha = \int_{\mathcal{U}} \mathbb{1}_{\{f(\mathbf{x}) > t\}} p(\mathbf{x}) d\mathbf{x} + \int_{\mathcal{X} \setminus \mathcal{U}} \mathbb{1}_{\{f(\mathbf{x}) > t\}} p(\mathbf{x}) d\mathbf{x},$$

inspiring an equivalent formulation of the surrogate MC estimator,

$$\hat{\alpha}_{\text{SURR}} = \frac{1}{M} \left[ \sum_{\mathbf{x}_i \in \mathcal{U}} \mathbb{1}_{\{\mu_n(\mathbf{x}_i) > t\}} + \sum_{\mathbf{x}_i \notin \mathcal{U}} \mathbb{1}_{\{\mu_n(\mathbf{x}_i) > t\}} \right] \quad \text{for } \mathbf{x}_i \stackrel{\text{iid}}{\sim} p(\mathbf{x}).$$

Now for  $\mathbf{x}_i \in \mathcal{U}$ , we upgrade surrogate prediction  $\mu_n(\mathbf{x}_i)$  to expensive evaluation of the true  $f(\mathbf{x}_i)$ , resulting in the following “hybrid MC” estimator:

$$\hat{\alpha}_{\text{HYB}} = \frac{1}{M} \left[ \sum_{\mathbf{x}_i \in \mathcal{U}} \mathbb{1}_{\{f(\mathbf{x}_i) > t\}} + \sum_{\mathbf{x}_i \notin \mathcal{U}} \mathbb{1}_{\{\mu_n(\mathbf{x}_i) > t\}} \right] \quad \text{for } \mathbf{x}_i \stackrel{\text{iid}}{\sim} p(\mathbf{x}). \quad (7)$$

The hybrid nature of this estimator is in the use of both true simulator evaluations (left term) and surrogate evaluations (right term). The accuracy of this estimator is contingent upon the classification accuracy of the surrogate and the choice of  $\mathcal{U}$ . If we restrict the size of  $\mathcal{U}$  so only  $B$ -many samples from  $X_M$  fall within it, i.e.,  $\sum_{i=1}^M \mathbb{1}_{\{\mathbf{x}_i \in \mathcal{U}\}} = B$ , then we can use this hybrid estimator while staying within our budgetary constraints. The evaluation of the expensive simulator at the Monte Carlo samples within  $\mathcal{U}$  constitutes the second stage of our design.

Rather than thinking of  $\mathcal{U}$  as a continuum, we find it easier to conceptualize in the context of the discrete set  $X_M$ . In a perfect world,  $\mathcal{U}$  would capture all the samples which the surrogate would misclassify. We are not privy to this information, and we are under a limited budget, but we can leverage the surrogate’s UQ to identify the  $B$ -many samples at which it is most uncertain. Recall, classification entropy (5) quantifies the degree of uncertainty in the pass/fail prediction of a surrogate. Consequently, our proposed allocation of samples to  $\mathcal{U}$  is strikingly simple – place the  $B$ -many samples from  $X_M$  with the highest entropy into  $\mathcal{U}$ . Denote these as  $X_M^B$ . Revisiting Figure 3, notice the high entropy regions (green) align well with the misclassification regions (yellow shading). The entropy criterion is effectively identifying regions of high classification uncertainty where we could most utilize expensive true simulator evaluations to correct inaccurate surrogate classifications.

Ultimately, after completing the second design stage by evaluating  $f(\mathbf{x})$  for  $\mathbf{x} \in X_M^B$ , we update the surrogate with these additional observations, thereby updating  $\mu_n(\mathbf{x})$ , before returning  $\hat{\alpha}_{\text{HYB}}$  (7). The process of observing the true simulator at the high entropy locations and updating the surrogate accordingly could be done in small batches within a feedback loop as demonstrated in Figure 1. Yet in our exercises, we have not seen smaller batch sizes to improve performance (we provide empirical evidence of this in Supplementary Material). Accordingly, we prefer to collect a single batch of all  $B$ -many high entropy samples at once.

### 3.3 Summary and related work

We have presented a comprehensive strategy for estimating Eq. (1) from a budget of size  $N$ . It is summarized as follows. Start with a very large Monte Carlo sample from  $p(\mathbf{x})$ , denoted  $X_M$ . Train a surrogate model through a contour locating sequential design, monitoring the progress of the  $\hat{\alpha}_{\text{SURR}}$  estimate (4) for given  $X_M$ , and halting contour location once two consecutive updates are within  $\pm \hat{\sigma}_\alpha$ . Denote the design points chosen in this stage as  $X_n$ . Then, use the trained surrogate to identify the highest entropy samples,  $X_M^B$ , evaluate the simulator at these inputs, and update the surrogate with these new observations. Finally, return  $\hat{\alpha}_{\text{HYB}}$  following Eq. (7).

Given the deterministic nature of  $f(\mathbf{x})$ , effective surrogates should interpolate observed points, i.e.,  $\mu_n(\mathbf{x}_i) = f(\mathbf{x}_i)$  when the surrogate has been trained on  $\{\mathbf{x}_i, y_i\}$ . In this light, the hybrid MC estimator (7) is akin to a surrogate MC estimator (4) when the surrogate has been trained on all  $\mathbf{x}_i \in \mathcal{U}$ . This connection permits us to frame our contribution as a *two-stage design*. In the first stage,  $X_n$  is chosen over  $\mathcal{X}$  based on contour location. In the second stage,  $X_M^B$  is chosen over  $\mathbb{P}_{\mathbf{x}}$  based on maximum entropy. The final design of size  $N$  is then  $X_N = [X_n^\top, X_M^B]^\top$ .

There are some noteworthy distinctions between these two design stages, as depicted in Figure 1. In the first stage, the  $n$  points selected for contour location may be acquired anywhere in the domain  $\mathcal{X}$ ,

seeking to balance both exploration of the response surface and exploitation of the suspected contour. In fact, the contour locating sequential design strategies we consider in Section 4 (Cole et al., 2023; Booth et al., 2024c) intentionally circumvent acquisitions based on maximal entropy in order to avoid clustered acquisitions and to promote more exploration of the surface. Alternatively, the  $B$  points chosen in the second stage must originate from  $p(\mathbf{x})$  and are solely exploitative. By nature, they will be clustered around the predicted contour, where pass/fail classifications are hardest to pin down. We contend that having a mix of data from these two realms is superior to either extreme.

Some of the previous works referenced in Section 1 have investigated stopping criteria for surrogate training in reliability settings. The most similar to our proposed criterion is that of Zhu and Du (2016) who recommend a convergence criterion akin to  $\frac{\hat{\sigma}_\alpha}{\alpha} \leq \epsilon$ , where  $\epsilon$  is a user-specified threshold. While similar to our stopping criterion, the choice of  $\epsilon$  here is make-or-break, and little guidance is provided. If  $\epsilon$  is too high, contour location will be halted too soon; if too low, contour location will continue past the point of utility. Our proposed stopping criterion avoids this choice and may be easily automated without problem-specific tuning. In our synthetic experiments, we find that it consistently results in appropriate termination with budget to spare.

Hybrid MC estimators (similar to Eq. 7) have been entertained in other settings. Li and Xiu (2010) use polynomial chaos models for a hybrid MC estimator with samples allocated to  $\mathcal{U}$  based on predicted proximity to the contour, i.e.,  $|\mu_n(\mathbf{x}_i) - t|$ . Their work, however, does not consider surrogate design and does not leverage surrogate UQ. Fuhrlander and Schöps (2020) use hybrid MC, but they only consider training the surrogate on samples from  $p(\mathbf{x})$ . Echard et al. (2011) similarly train only on a subset of  $X_M$ . We attempted to recreate the approach of Fuhrlander and Schöps (2020) in our setting: (i) sample large  $X_M$ , (ii) train an initial surrogate on a random selection of these samples, (iii) use the surrogate with a metric such as entropy to select additional batches from  $X_M$  for evaluation through the simulator, (iv) update the surrogate, and (v) repeat steps (iii)-(iv) until the budget is exhausted. Yet we were unable to obtain even reasonable results because initial surrogate fits were very poor, and surrogate-informed acquisitions were unable to recover. Random selections from  $X_M$  were overwhelmingly in high probability regions, not low probability failure regions. Hristov et al. (2019) noticed this conundrum and stated it well: “using a surrogate that is built on frequent events to predict and analyze rare events” can be futile.

To visualize this conundrum in a simple setting, we revisit the Herbie example of Figure 2. With the input distribution centered at the origin, the probability of generating any samples outside  $[-1, 1]^2$  is very low. But a GP surrogate would benefit from some “anchor points” in these outer regions (Gramacy and Apley, 2015). This distinction will be less prominent if  $p(\mathbf{x})$  is uniformly distributed over  $\mathcal{X}$ , but the trade-off between exploring in Stage 1 and exploiting in Stage 2 will still be impactful. Even with uniform  $p(\mathbf{x})$ , training a surrogate only on maximal entropy points is suboptimal (Cole et al., 2023; Booth et al., 2024c).

## 4 Synthetic experiments

In this section we benchmark our method against state-of-the-art competitors on a variety of synthetic experiments. We consider four functions: the 2d Herbie function (Lee et al., 2011) with a total budget of 150, the 3d Ishigami function (Ishigami and Homma, 1990) with a total budget of 300, the 6d Hartmann function (Picheny et al., 2013) with a total budget of 600, and the 4d Plateau function (Booth et al., 2024c) with a total budget of 200. The first three of these are plausibly stationary, so we use a standard GP surrogate, fit with the `Scikit-learn` package in `python` (Pedregosa et al., 2011), and the entropy contour location scheme of Cole et al. (2023). The Plateau function is known to be nonstationary; it is characterized by flat regions with a steep sloping drop between them. To address the nonstationarity, we

use a Bayesian DGP surrogate (Sauer et al., 2023b), fit with the `deepgp` package in R (Booth, 2024), and the contour location scheme of Booth et al. (2024c). With the right surrogate, the failure contour of the Plateau function can be well estimated from a rather small amount of data.

Function	True $\alpha$	$d$	$n_0$	$N$	$M$	Surrogate	CL Scheme
Herbie	$7.533 \times 10^{-5}$	2	20	150	$3.5 \times 10^7$	GP	Cole et al. (2023)
Ishigami	$1.904 \times 10^{-4}$	3	50	300	$1.5 \times 10^7$	GP	Cole et al. (2023)
Hartmann	$1.001 \times 10^{-5}$	6	100	600	$1.0 \times 10^8$	GP	Cole et al. (2023)
Plateau	$4.308 \times 10^{-4}$	4	30	200	$3.5 \times 10^6$	DGP	Booth et al. (2024c)

Table 1: Simulation settings. True  $\alpha$  values are estimated from 10 billion samples.

Table 1 summarizes the simulation settings. Functions are observed without noise to mimic a deterministic computer simulation. We define failure thresholds and input distributions for each function, resulting in the failure probabilities reported in Table 1. All input distributions are variations/combinations of independent uniform and truncated normal distributions; further details of the functions, thresholds, and distributions are reserved for Supplementary Material. We choose  $M$  for each  $\alpha$  to keep  $\sigma_\alpha$  conservatively under 5%.

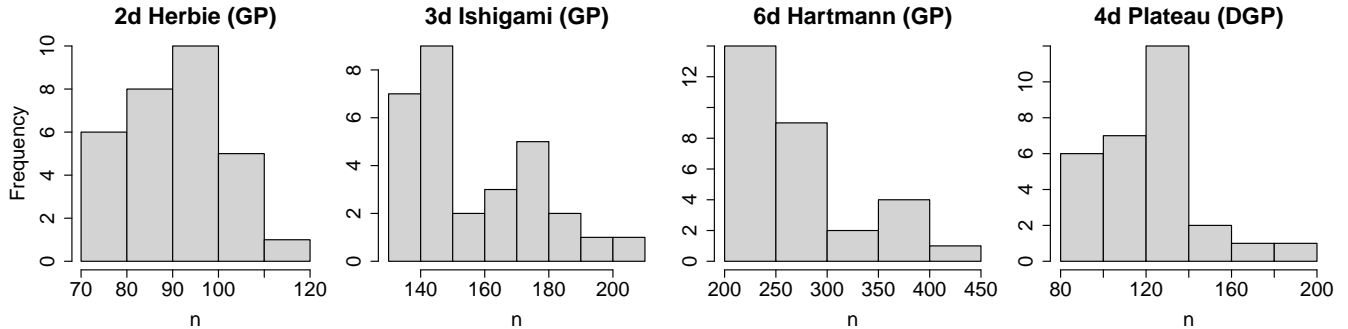


Figure 5: Distribution of the chosen  $n$  across 30 repetitions.

First, we deploy our stopping criterion (Section 3.1) for each of the four scenarios (Table 1). Starting with an initial LHS sample of size  $n_0$ , we proceed with Stage 1, conducting CL with the specified method and determining the  $n$  at which to stop. We conduct 30 re-randomized Monte Carlo repetitions. To avoid premature termination, we require a minimum of 10 observed failures and  $n \geq 2n_0$  (at least as many contour locating acquisitions as original space-filling observations). Figure 5 shows the distribution of chosen  $n$  values for each scenario. Notice, all trials terminated before the allotted  $N$ , reserving some evaluations for Stage 2, but there was considerable variability across trials. We view this variability as a strength – some random initializations need more data to effectively locate the contour while some get lucky from the start. Allowing the surrogate to dictate its own budget allocation mitigates some of the risks of having an unlucky starting design.

For each trained surrogate with chosen  $n$  (which varies across repetitions), we collect a large Monte Carlo sample ( $X_M$ , constant across methods, randomized across repetitions), then compare the following estimation methods. All variations use the same Stage 1 contour location scheme up to point  $n$ ; they differ only in their use of the remaining  $B = N - n$  observations.

- Exhaustive CL: Ignoring the chosen  $n$ , continue contour location until the entire budget is exhausted and return the surrogate MC estimate (4).

- Two-stage Entropy: Our **proposed** two-stage approach (Figure 1) using the hybrid MC estimate (7) where  $\mathcal{U}$  is chosen to contain the  $B$  points from  $X_M$  with highest entropy.
- Two-stage Proximity: Same as “Two-stage Entropy,” but  $\mathcal{U}$  is chosen to contain the  $B$  points from  $X_M$  which are predicted to be closest to the failure threshold (i.e., the samples with the smallest  $|\mu_n(\mathbf{x}_i) - t|$ ). This is inspired by the work of [Li and Xiu \(2010\)](#).
- SIIS: Surrogate-informed importance sampling (6), with  $B$ -many samples observed from an estimated GMM bias distribution ([Peherstorfer et al., 2016](#)). The bias distribution is trained on the predicted failures, i.e.,  $\{\mathbf{x}_i \in X_M \mid \mu_n(\mathbf{x}_i) > t\}$ . For our GP surrogates implemented in `python`, we use the `scikit-learn` package ([Pedregosa et al., 2011](#)) to train GMM bias distributions. For our DGP surrogates implemented in `R`, we use the `mclust` package ([Scrucca et al., 2016](#)).
- SIIS UCB: Same as “SIIS,” but the bias distribution is trained on the samples whose upper 95% confidence bound exceeds the threshold, i.e.,  $\{\mathbf{x}_i \in X_M \mid \mu_n(\mathbf{x}_i) + 1.645\sigma_n(\mathbf{x}_i) > t\}$ .

As implemented, the latter three are to some degree an internal comparison since they use our proposed stopping criterion to determine the budget allocation between surrogate training ( $n$ ) and estimation ( $B$ ). Without borrowing from our proposed approach, there would be no guidance on the allocation of  $n$  and  $B$  for these methods. The “Two-stage Proximity” approach is truly an internal comparison as it borrows everything from our proposed two-stage design aside from the specific allocation of samples to  $\mathcal{U}$ . It is included to show the impact of the entropy selection criterion, which uses surrogate UQ, over a selection solely based on the posterior mean. Reproducible code for all experiments, including both the `python` and `R` implementations, is available in our public git repository.<sup>2</sup>

Results are shown in Figure 6. Red dashed lines mark the true failure probabilities, and grey shaded regions highlight  $\{\alpha \pm 2\sigma_\alpha\}$  where  $\sigma_\alpha$  is calculated from the true  $\alpha$  and chosen  $M$ . This region provides important context – it captures the intrinsic variability that would accompany any MC estimator. In other words, even if we used the true simulator for all  $\{\mathbf{x}_i\}_{i=1}^M$  samples (2), we would obtain a boxplot roughly spanning the grey interval. We thus consider any results within this region to be effective estimates. We could tighten the interval (and the boxplots of the MC methods) by increasing  $M$  without requiring any additional simulator evaluations, another advantage MC holds over IS.

Across the board, both importance sampling based methods (“SIIS” and “SIIS UCB”) suffered from high variability in their failure probability estimates. Although their median performance was generally on target (indicative of their unbiasedness), these methods consistently offered the poorest performance. The more conservative “SIIS UCB” had no apparent advantage over the traditional “SIIS.” We believe importance sampling is simply ill-suited for our low data settings. In all scenarios aside from the simplest two-dimensional Herbie function (where performance was comparable), our two-stage design (“Two-stage Entropy”) outperformed the exhaustive contour location approach (“Exhaustive CL”). Particularly as dimension grows and the response surface becomes more complex, there is a clear advantage to our two-stage design which transitions from CL to exploitation of MC samples. Within the two-stage designs, there was generally agreement between the two variations we considered for allocating samples to  $\mathcal{U}$  (“Entropy” and “Proximity”), but when there was disagreement the entropy criterion offered higher accuracy, with uniformly superior worst-case performance. As suspected, the entropy criterion which incorporates uncertainty is more effective at identifying samples which the surrogate would misclassify.

---

<sup>2</sup><https://bitbucket.org/boothlab/failprob/>

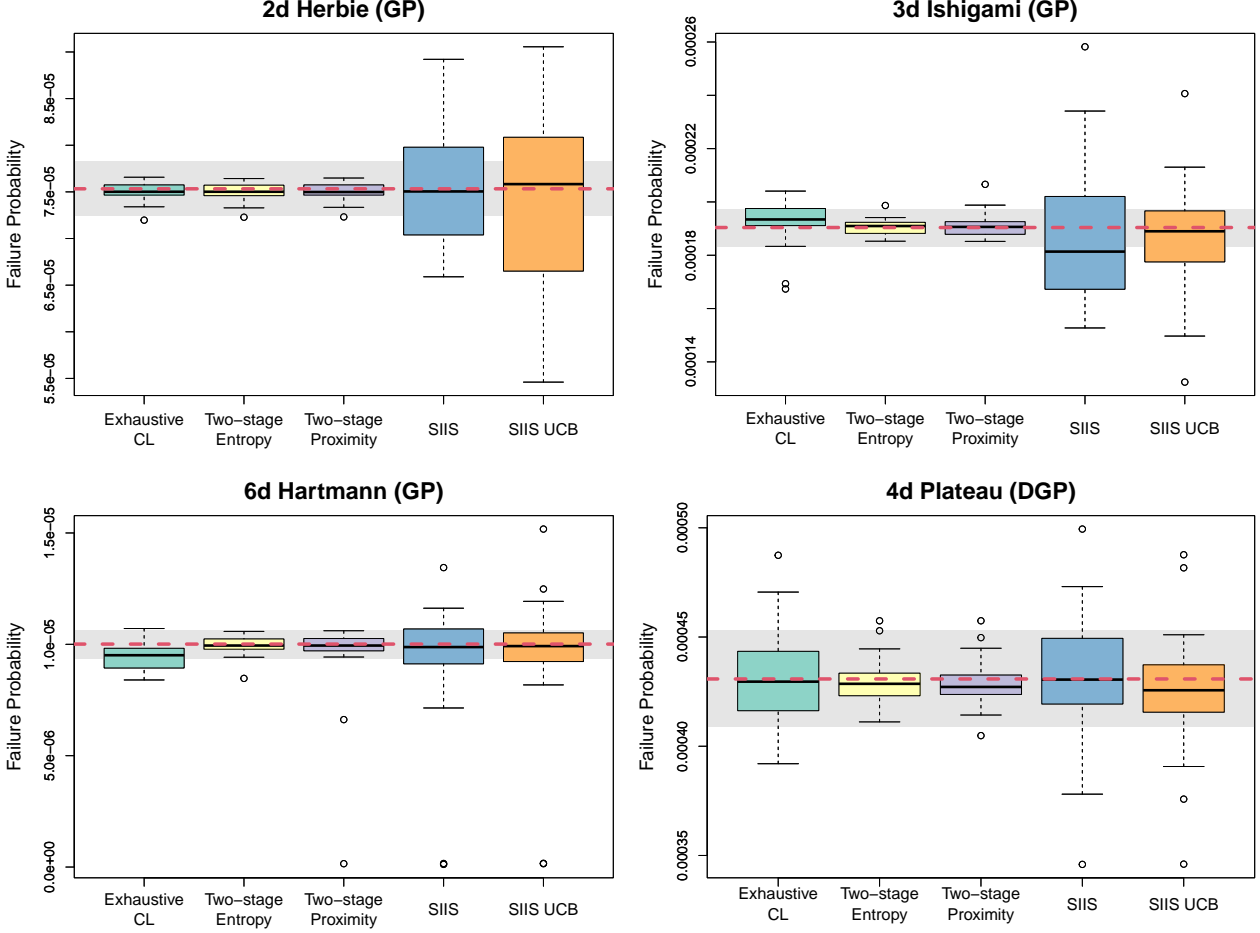


Figure 6: Estimated failure probabilities shown over true failure probability (red dashed)  $\pm 2$  standard errors (grey shading). Boxplots show 30 repetitions.

## 5 RAE-2822 airfoil computer experiment

The RAE-2822 airfoil computer experiment simulates the flow of air around an aircraft wing. The simulation suite is solved via SU2, and the software is publicly available (Economou et al., 2016). We consider seven inputs: four shape parameters ( $S_i$  for  $i = 1, \dots, 4$ ) and 3 environmental parameters, namely angle of attack, Reynolds number, and Mach number. We are interested in the lift over drag ( $L/D$ ) ratio.  $L/D$  values that are too low represent inefficient aircraft performance. We define a failure threshold at  $t = 3$  such that  $L/D < 3$  indicates failure. [Note the change from  $f(\mathbf{x}) > t$  to  $f(\mathbf{x}) < t$  does not affect the implementation of our method.] This computer experiment requires nearly 30 minutes of compute time with serial execution, but reductions are possible with parallel execution.

Our objective is to estimate the probability of failure given the following input distribution:

$$S_i \sim \text{Unif}(-1 \times 10^{-4}, 1 \times 10^{-4}) \text{ for } i = 1, \dots, 4$$

Angle of Attack  $\sim \mathcal{N}(\mu = 5, \sigma = 1)$  truncated to  $[0, 10]$

Reynolds number  $\sim \mathcal{N}(\mu = 1 \times 10^7, \sigma = 1 \times 10^6)$  truncated to  $[5 \times 10^6, 1.5 \times 10^7]$

Mach number  $\sim \mathcal{N}(\mu = 0.8, \sigma = 0.02)$  truncated to  $[0.7, 0.9]$ .

We fix our total budget at  $N = 500$  simulator evaluations and use  $M = 2.5 \times 10^6$  for the size of  $X_M$ . Booth et al. (2024c) found that DGP surrogates outperformed GP surrogates for contour location of this experiment. We follow the settings therein, starting with an LHS sample of size  $n_0 = 100$  and fitting a Bayesian DGP surrogate with the `deepgp` package. We proceed with contour location (Stage 1) following Booth et al. (2024c), stopping after every 10th acquisition to estimate  $\hat{\alpha}$  and check whether it is within the  $\pm \hat{\sigma}_\alpha$  bounds. Once we halt contour location (Section 3.1), we proceed to Stage 2, using entropy to inform our hybrid MC estimator (Section 3.2). Given the larger input dimension, we require at least 40 observed failures before we consider halting surrogate training. Since the true failure probability is unknown, we opt to repeat this entire exercise twice, with a newly randomized starting design. We consider the agreement between the two randomized repetitions as an indication that our procedure is well-calibrated.

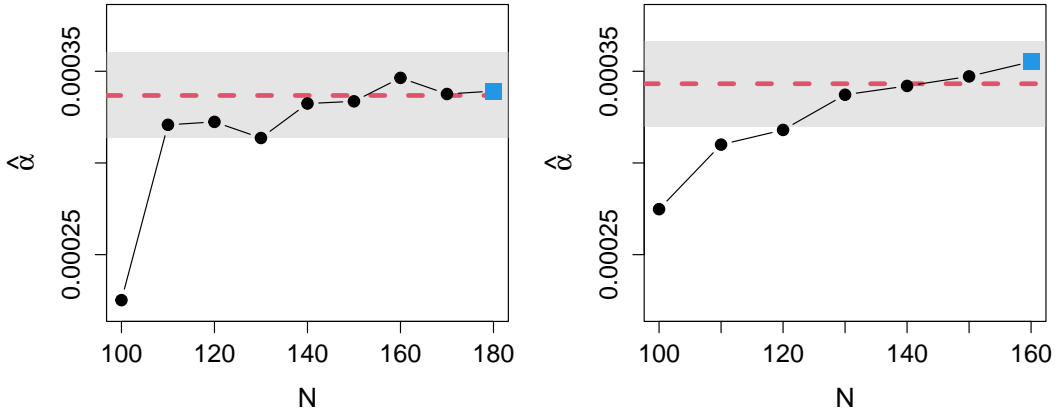


Figure 7: Progress in  $\hat{\alpha}$  across two contour locating designs for the airfoil computer experiment. Proposed two-stage failure probability estimate shown in dashed red. Grey shading indicates  $\hat{\alpha} \pm 2\hat{\sigma}_\alpha$  for these final estimates. Left/right panels show two repetitions with newly randomized starting designs.

Figure 7 reports the progress in  $\hat{\alpha}$  over the course of each design. Our stopping criterion halted the sequential designs at  $n = 180$  and  $n = 160$ , leaving  $B = 320$  and  $B = 340$  for the second design stage, respectively. Our two hybrid Monte Carlo estimates were  $\hat{\alpha}_{\text{HYB}} = \{0.0003368, 0.0003432\}$ . These values are indicated by the red dashed lines in Figure 7. The grey shading shows  $\hat{\alpha} \pm 2\hat{\sigma}_\alpha$ , calculated from these final estimates. Although the two estimates vary slightly, they are both within the bounds of reasonable variability for our chosen  $M$ . Additionally, notice how the final hybrid MC estimate of the second exercise (right panel) brought the failure probability lower than what the surrogate had originally estimated, closer to the estimate of our first attempt (left panel). We take this as an indication that the hybrid estimator of Stage 2 is effectively adjusting for surrogate inaccuracies remaining after Stage 1.

## 6 Discussion

We presented a unique two-stage surrogate design for estimating failure probabilities of expensive computer experiments, which outperforms both exhaustive contour location and surrogate-informed importance sampling. Starting with a contour locating sequential design, we halt contour location once surrogate training has plateaued, as indicated by practical convergence of a surrogate Monte Carlo estimator. Then we use the remaining budget of simulator evaluations on the Monte Carlo samples with highest entropy, to ultimately return a hybrid MC estimate of  $\alpha$ . Our design strategically leverages the uncertainty quantification

provided by the surrogate to reserve expensive simulator evaluations for samples with high classification uncertainty. While we limited our experiments to GP and DGP surrogates, our proposed scheme is applicable to any surrogate which provides posterior predictive distributions (which are required for entropy calculations). Extensions to other surrogates, such a treed Gaussian processes (Gramacy and Lee, 2008) or Bayesian additive regression trees (Chipman et al., 2010), is straightforward.

Our two-stage design is computationally efficient in the number of evaluations of the expensive simulator, but it requires many predictive evaluations from the surrogate. While surrogate predictions are very cheap, collecting billions of them is not necessarily trivial. The computational cost of obtaining these predictions increases with  $n/N$ ,  $d$ , and  $M$ , but it also depends on the surrogate and computing environment. For context, the most expensive predictions we needed in our exercises were those of our motivating airfoil simulator, with the fully-Bayesian DGP trained on all  $N = 500$  points in 7-dimensions. With parallelization over 10 CPUs, it took just over 10 minutes to obtain one million predictions. For smaller  $\alpha$  requiring  $M$  in the billions, the cost of these surrogate predictions may present an obstacle, but it is still far cheaper than comparative evaluations of the true expensive computer simulator.

There may be avenues to circumvent surrogate predictions at all  $X_M$  locations. We hypothesize that a classification rule based on nearest neighbors could work well: for a particular  $\mathbf{x}_i$ , if the surrogate predicts that all of its  $k$ -many nearest neighbors are “passes,” then we could presume  $\mathbb{1}_{\{\mu_n(\mathbf{x}_i) > t\}} = 0$  without needing to obtain  $\mu_n(\mathbf{x}_i)$  directly. This requires effective tuning of  $k$ , and would only speed-up computations if the cost of obtaining the nearest neighbor sets is less than that of obtaining the single surrogate prediction. For these reasons, we did not entertain such workarounds in our current work.

In all of our examples, our stopping criterion terminated contour location before the complete budget ( $N$ ) was exhausted. If a simulation budget is severely restricted, the budget could be exhausted before our proposed stopping criterion is met. While we prefer to have additional evaluations reserved for Stage 2, we contend that using the entire budget for contour location in Stage 1 to inform a traditional surrogate MC estimate is the best option in this scenario. As we’ve shown, importance sampling based methods perform poorly when data is limited.

We have exclusively focused on deterministic computer experiments. In fact, the noise-free nature of the simulator is what enabled us to frame our contribution as a two-stage design. Once  $f(\mathbf{x}_i)$  has been observed and incorporated into the surrogate, surrogate predictions should interpolate these observations. Thus our hybrid MC estimator (7) is really a surrogate MC estimator (4), with a strategically trained surrogate. Stochastic simulators (e.g., Baker et al., 2022) present a unique challenge as repeated observations of noisy  $f(\mathbf{x})$  may result in a mix of passes and failures for the same  $\mathbf{x}$ . To accommodate this, we could have broadened the formulation of Eq. (1) by replacing the indicator function  $\mathbb{1}_{\{f(\mathbf{x}) > t\}}$  with the unknown probability  $P(f(\mathbf{x}) > t)$ , which recovers the indicator when  $f$  is deterministic. The key advantage of our hybrid estimator – that observing  $f(\mathbf{x}_i)$  ensures correct classification of  $\mathbb{1}_{\{f(\mathbf{x}_i) > t\}}$  – is not applicable to noisy simulators. Instead, new active learning strategies that strategically allocate replicates (Binois et al., 2019) and inform a MC estimator leveraging surrogate posterior predictive probabilities are warranted. We leave this as an avenue for future work.

When the input distribution is not uniform over  $\mathcal{X}$ , it could be beneficial to leverage information about  $p(\mathbf{x})$  in the sequential training of the surrogate (Abdelmalek-Lomenech et al., 2024). There is arguably no need to train a surrogate in a region where inputs will never occur. Incorporating this information in the contour location stage could improve failure probability estimation downstream, but we have seen positive impacts from having “anchor points” in regions of very low density (such as those around the edges in Figure 2). We suspect there is a delicate balance that would work well here, but this avenue is currently underexplored. Furthermore, while we focused on stochastic inputs, it is possible to extend our approach to incorporate controllable/design variables by using point masses in  $p(\mathbf{x})$ .

Finally, estimation of failure probabilities is often an intermediate step within a larger objective, such as a stochastically constrained optimization. For example, in the context of our airfoil experiment, we may wish to find the optimal wing configuration given that the probability of failure remains below a specified threshold. The ability to effectively estimate failure probabilities from limited data, which we have tackled here, is integral to the success of this larger enterprise. While we focused on allocating a predetermined budget of evaluations, it could be useful to develop a decision rule for halting Stage 2, potentially reserving some evaluations, particularly if this design is within a larger optimization loop.

## References

Abdelmalek-Lomenech, R. A., Bect, J., Chabridon, V., and Vazquez, E. (2024). “Bayesian sequential design of computer experiments for quantile set inversion.” *Technometrics*, , just-accepted, 1–14.

Au, S.-K. and Beck, J. L. (2001). “Estimation of small failure probabilities in high dimensions by subset simulation.” *Probabilistic engineering mechanics*, 16, 4, 263–277.

Azzimonti, D., Ginsbourger, D., Chevalier, C., Bect, J., and Richet, Y. (2021). “Adaptive design of experiments for conservative estimation of excursion sets.” *Technometrics*, 63, 1, 13–26.

Baker, E., Barbillon, P., Fadikar, A., Gramacy, R. B., Herbei, R., Higdon, D., Huang, J., Johnson, L. R., Ma, P., Mondal, A., et al. (2022). “Analyzing stochastic computer models: A review with opportunities.” *Statistical Science*, 37, 1, 64–89.

Batet, L., Alvarez-Fernandez, J. M., de les Valls, E. M., Martinez-Quiroga, V., Perez, M., Reventos, F., and Sedano, L. (2014). “Modelling of a supercritical CO<sub>2</sub> power cycle for nuclear fusion reactors using RELAP5–3D.” *Fusion Engineering and Design*, 89, 4, 354–359.

Bect, J., Ginsbourger, D., Li, L., Picheny, V., and Vazquez, E. (2012). “Sequential design of computer experiments for the estimation of a probability of failure.” *Statistics and Computing*, 22, 773–793.

Belot, I., Vidal, D., Greiner, R., Votsmeier, M., Hayes, R. E., and Bertrand, F. (2021). “Impact of washcoat distribution on the catalytic performance of gasoline particulate filters as predicted by lattice Boltzmann simulations.” *Chemical Engineering Journal*, 406, 127040.

Bichon, B. J., Eldred, M. S., Swiler, L. P., Mahadevan, S., and McFarland, J. M. (2008). “Efficient global reliability analysis for nonlinear implicit performance functions.” *AIAA journal*, 46, 10, 2459–2468.

Binois, M., Huang, J., Gramacy, R. B., and Ludkovski, M. (2019). “Replication or exploration? Sequential design for stochastic simulation experiments.” *Technometrics*, 61, 1, 7–23.

Booth, A. S. (2024). *deepgp: Bayesian Deep Gaussian Processes using MCMC*. R package version 1.1.3.

Booth, A. S., Cooper, A., and Gramacy, R. B. (2024a). “Nonstationary Gaussian process surrogates.” *arXiv:2305.19242*.

Booth, A. S., Gramacy, R., and Renganathan, A. (2024b). “Actively learning deep Gaussian process models for failure contour and probability estimation.” In *AIAA SCITECH 2024 Forum*, 0577.

Booth, A. S., Renganathan, S. A., and Gramacy, R. B. (2024c). “Contour Location for Reliability in Airfoil Simulation Experiments using Deep Gaussian Processes.” *Annals of Applied Statistics*, , just-accepted. ArXiv:2308.04420.

Bugallo, M. F., Elvira, V., Martino, L., Luengo, D., Miguez, J., and Djuric, P. M. (2017). “Adaptive importance sampling: The past, the present, and the future.” *IEEE Signal Processing Magazine*, 34, 4, 60–79.

Cheng, K. and Lu, Z. (2020). “Structural reliability analysis based on ensemble learning of surrogate models.” *Structural Safety*, 83, 101905.

Cheng, K., Papaioannou, I., Lu, Z., Zhang, X., and Wang, Y. (2023). “Rare event estimation with sequential directional importance sampling.” *Structural Safety*, 100, 102291.

Chevalier, C., Bect, J., Ginsbourger, D., Vazquez, E., Picheny, V., and Richet, Y. (2014). “Fast parallel kriging-based stepwise uncertainty reduction with application to the identification of an excursion set.” *Technometrics*, 56, 4, 455–465.

Chipman, H. A., George, E. I., and McCulloch, R. E. (2010). “BART: Bayesian additive regression trees.” *The Annals of Applied Statistics*, 4, 1, 266 – 298.

Cole, D. A., Gramacy, R. B., Warner, J. E., Bomarito, G. F., Leser, P. E., and Leser, W. P. (2023). “Entropy-based adaptive design for contour finding and estimating reliability.” *Journal of Quality Technology*, 55, 1, 43–60.

Dalbey, K. R. and Swiler, L. P. (2014). “Gaussian process adaptive importance sampling.” *International Journal for Uncertainty Quantification*, 4, 2.

Damianou, A. and Lawrence, N. D. (2013). “Deep gaussian processes.” In *Artificial intelligence and statistics*, 207–215. PMLR.

Dubourg, V., Sudret, B., and Bourinet, J.-M. (2011). “Reliability-based design optimization using kriging surrogates and subset simulation.” *Structural and Multidisciplinary Optimization*, 44, 673–690.

Duhamel, C., Helbert, C., Munoz Zuniga, M., Prieur, C., and Sinoquet, D. (2023). “A SUR version of the Bichon criterion for excursion set estimation.” *Statistics and Computing*, 33, 2, 41.

Echard, B., Gayton, N., and Lemaire, M. (2011). “AK-MCS: an active learning reliability method combining Kriging and Monte Carlo simulation.” *Structural Safety*, 33, 2, 145–154.

Economou, T. D., Palacios, F., Copeland, S. R., Lukaczyk, T. W., and Alonso, J. J. (2016). “SU2: An open-source suite for multiphysics simulation and design.” *Aiaa Journal*, 54, 3, 828–846.

Fuhrländer, M. and Schöps, S. (2020). “A blackbox yield estimation workflow with Gaussian process regression applied to the design of electromagnetic devices.” *Journal of Mathematics in Industry*, 10, 1, 25.

Gramacy, R. B. (2020). *Surrogates: Gaussian Process Modeling, Design, and Optimization for the Applied Sciences*. CRC press.

Gramacy, R. B. and Apley, D. W. (2015). “Local Gaussian process approximation for large computer experiments.” *Journal of Computational and Graphical Statistics*, 24, 2, 561–578.

Gramacy, R. B. and Lee, H. K. H. (2008). “Bayesian treed Gaussian process models with an application to computer modeling.” *Journal of the American Statistical Association*, 103, 483, 1119–1130.

Gramacy, R. B., Sauer, A., and Wycoff, N. (2022). “Triangulation candidates for bayesian optimization.” *Advances in Neural Information Processing Systems*, 35, 35933–35945.

Haldar, A. and Mahadevan, S. (1995). “First-order and second-order reliability methods.” In *Probabilistic Structural Mechanics Handbook: theory and industrial applications*, 27–52. Springer.

Hristov, P., DiazDelaO, F., Farooq, U., and Kubiak, K. (2019). “Adaptive Gaussian process emulators for efficient reliability analysis.” *Applied Mathematical Modelling*, 71, 138–151.

Huang, X., Chen, J., and Zhu, H. (2016). “Assessing small failure probabilities by AK–SS: An active learning method combining Kriging and Subset Simulation.” *Structural Safety*, 59, 86–95.

Ishigami, T. and Homma, T. (1990). “An importance quantification technique in uncertainty analysis for computer models.” In [1990] *Proceedings. First international symposium on uncertainty modeling and analysis*, 398–403. IEEE.

Joseph, V. R. (2016). “Space-filling designs for computer experiments: A review.” *Quality Engineering*, 28, 1, 28–35.

Kurtz, N. and Song, J. (2013). “Cross-entropy-based adaptive importance sampling using Gaussian mixture.” *Structural Safety*, 42, 35–44.

Lee, H., Gramacy, R., Linkletter, C., and Gray, G. (2011). “Optimization subject to hidden constraints via statistical emulation.” *Pacific Journal of Optimization*, 7, 3, 467–478.

Li, J. and Xiu, D. (2010). “Evaluation of failure probability via surrogate models.” *Journal of Computational Physics*, 229, 23, 8966–8980.

Li, M., Wang, G., Qian, L., Li, X., and Ma, Z. (2021). “ASS-GPR: Adaptive Sequential Sampling Method Based on Gaussian Process Regression for Reliability Analysis of Complex Geotechnical Engineering.” *International Journal of Geomechanics*, 21, 10, 04021192.

Lu, N., Li, Y.-F., Huang, H.-Z., Mi, J., and Niazi, S. G. (2023). “AGP-MCS+ D: An active learning reliability analysis method combining dependent Gaussian process and Monte Carlo simulation.” *Reliability Engineering & System Safety*, 240, 109541.

MacKay, D. J. (1995). “Bayesian neural networks and density networks.” *Nuclear Instruments and Methods in Physics Research Section A: Accelerators, Spectrometers, Detectors and Associated Equipment*, 354, 1, 73–80.

Marques, A., Lam, R., and Willcox, K. (2018). “Contour location via entropy reduction leveraging multiple information sources.” *Advances in neural information processing systems*, 31.

McKay, M. D., Beckman, R. J., and Conover, W. J. (2000). “A comparison of three methods for selecting values of input variables in the analysis of output from a computer code.” *Technometrics*, 42, 1, 55–61.

Mia, M. S., Islam, M. S., and Ghosh, U. (2017). “Modal analysis of cracked cantilever beam by finite element simulation.” *Procedia engineering*, 194, 509–516.

Ming, D., Williamson, D., and Guillas, S. (2023). “Deep Gaussian process emulation using stochastic imputation.” *Technometrics*, 65, 2, 150–161.

Oh, M.-S. and Berger, J. O. (1992). “Adaptive importance sampling in Monte Carlo integration.” *Journal of statistical computation and simulation*, 41, 3-4, 143–168.

O’Hagan, A. (1987). “Monte Carlo is fundamentally unsound.” *The Statistician*, 247–249.

Park, C., Haftka, R. T., and Kim, N. H. (2017). “Remarks on multi-fidelity surrogates.” *Structural and Multidisciplinary Optimization*, 55, 1029–1050.

Pedregosa, F., Varoquaux, G., Gramfort, A., Michel, V., Thirion, B., Grisel, O., Blondel, M., Prettenhofer, P., Weiss, R., Dubourg, V., et al. (2011). “Scikit-learn: Machine learning in Python.” *the Journal of machine Learning research*, 12, 2825–2830.

Peherstorfer, B., Cui, T., Marzouk, Y., and Willcox, K. (2016). “Multifidelity importance sampling.” *Computer Methods in Applied Mechanics and Engineering*, 300, 490–509.

Picheny, V., Wagner, T., and Ginsbourger, D. (2013). “A benchmark of kriging-based infill criteria for noisy optimization.” *Structural and multidisciplinary optimization*, 48, 607–626.

Rajaram, D., Puranik, T. G., Ashwin Renganathan, S., Sung, W., Fischer, O. P., Mavris, D. N., and Ramamurthy, A. (2021). “Empirical assessment of deep gaussian process surrogate models for engineering problems.” *Journal of Aircraft*, 58, 1, 182–196.

Ranjan, P., Bingham, D., and Michailidis, G. (2008). “Sequential experiment design for contour estimation from complex computer codes.” *Technometrics*, 50, 4, 527–541.

Rasmussen, C. E., Williams, C. K., et al. (2006). *Gaussian Processes for Machine Learning*, vol. 1. Springer.

Renganathan, A. (2024). “Efficient reliability analysis with multifidelity Gaussian processes and normalizing flows.” In *AIAA SCITECH 2024 Forum*, 0576.

Renganathan, S. A., Rao, V., and Navon, I. M. (2023). “CAMERA: A method for cost-aware, adaptive, multifidelity, efficient reliability analysis.” *Journal of Computational Physics*, 472, 111698.

Reynolds, D. A. et al. (2009). “Gaussian mixture models.” *Encyclopedia of biometrics*, 741, 659-663.

Santner, T. J., Williams, B. J., and Notz, W. I. (2018). *The Design and Analysis of Computer Experiments*. Springer.

Sauer, A. (2023). “Deep Gaussian process surrogates for computer experiments.” Ph.D. thesis, Virginia Polytechnic Institute and State University.

Sauer, A., Cooper, A., and Gramacy, R. B. (2023a). “Vecchia-approximated deep Gaussian processes for computer experiments.” *Journal of Computational and Graphical Statistics*, 32, 3, 824–837.

Sauer, A., Gramacy, R. B., and Higdon, D. (2023b). “Active learning for deep Gaussian process surrogates.” *Technometrics*, 65, 4–18.

Scrucca, L., Fop, M., Murphy, T. B., and Raftery, A. E. (2016). “mclust 5: clustering, classification and density estimation using Gaussian finite mixture models.” *The R Journal*, 8, 1, 289–317.

Srinivasan, R. (2002). *Importance Sampling: Applications in Communications and Detection*. Springer Science & Business Media.

Su, G., Peng, L., and Hu, L. (2017). “A Gaussian process-based dynamic surrogate model for complex engineering structural reliability analysis.” *Structural Safety*, 68, 97–109.

Tabandeh, A., Jia, G., and Gardoni, P. (2022). “A review and assessment of importance sampling methods for reliability analysis.” *Structural Safety*, 97, 102216.

Tokdar, S. T. and Kass, R. E. (2010). “Importance sampling: a review.” *Wiley Interdisciplinary Reviews: Computational Statistics*, 2, 1, 54–60.

Yazdi, F. (2022). “Fast deep gaussian process modeling and design for large complex computer experiments.” Ph.D. thesis, Simon Fraser University.

Zhang, L., Lu, Z., and Wang, P. (2015). “Efficient structural reliability analysis method based on advanced Kriging model.” *Applied Mathematical Modelling*, 39, 2, 781–793.

Zhu, Z. and Du, X. (2016). “Reliability analysis with Monte Carlo simulation and dependent Kriging predictions.” *Journal of Mechanical Design*, 138, 12, 121403.

# SUPPLEMENTARY MATERIAL

## A Test functions

Here we provide the details of the functions, thresholds, and input distributions used in the benchmark exercises of Section 4. In each case, failures are defined as  $f(\mathbf{x}) > t$ .

**Herbie.** The 2d Herbie function (Lee et al., 2011) is defined in over  $[-2, 2]^2$  as

$$f(\mathbf{x}) = \prod_{i=1}^2 \exp(-(x_i - 1)^2) + \exp(-0.8 * (x_i + 1)^2) - 0.05 * \sin(8 * (x_i + 1)).$$

We set the failure threshold at  $t = 1.065$  and define the input distribution as  $x_i \stackrel{\text{ind}}{\sim} \mathcal{N}(0, 0.36)$  for  $i = 1, 2$ , truncated to  $[-2, 2]$ .

**Ishigami.** The 3d Ishigami function (Ishigami and Homma, 1990) is defined over  $[-\pi, \pi]^3$  as

$$f(\mathbf{x}) = \sin(x_1) + 5 * \sin(x_2)^2 + 0.1 * x_3^4 * \sin(x_1).$$

We set the failure threshold at  $t = 10.244$  and define the input distribution as

$$\begin{aligned} x_1 &\sim \mathcal{N}(-1, 1) \text{ truncated to } [-\pi, \pi] \\ x_2 &\sim \mathcal{N}(1.5, 1.5) \text{ truncated to } [-\pi, \pi] \\ x_3 &\sim \text{Uniform}(-\pi, \pi). \end{aligned}$$

**Hartmann.** The 6d Hartmann function (Picheny et al., 2013) is defined over  $[0, 1]^6$  as

$$f(\mathbf{x}) = - \sum_{i=1}^4 \alpha_i \exp \left( - \sum_{j=1}^6 A_{ij} (x_j - P_{ij})^2 \right) \text{ where}$$

$$\alpha^\top = \begin{bmatrix} 1 \\ 1.2 \\ 3 \\ 3.2 \end{bmatrix} \quad A^\top = \begin{bmatrix} 10 & .05 & 3 & 17 \\ 3 & 10 & 3.5 & 8 \\ 17 & 17 & 1.7 & .05 \\ 3.5 & .1 & 10 & 10 \\ 7 & 8 & 17 & .1 \\ 8 & 14 & 8 & 14 \end{bmatrix} \quad \text{and} \quad P^\top = \begin{bmatrix} .1312 & .2329 & .2348 & .4047 \\ .1696 & .4135 & .1451 & .8828 \\ .5569 & .8307 & .3522 & .8732 \\ .0124 & .3736 & .2883 & .5743 \\ .8283 & .1004 & .3047 & .1091 \\ .5886 & .9991 & .6650 & .0381 \end{bmatrix}.$$

We set the failure threshold at  $t = 2.46$  and define the input distribution as  $x_i \stackrel{\text{ind}}{\sim} \mathcal{N}(0.5, 0.1)$  for  $i = 1, \dots, 6$ , truncated to  $[0, 1]$ .

**Plateau.** The Plateau function (Booth et al., 2024c) is defined in arbitrary dimension over  $[0, 1]^d$  as

$$f(\mathbf{x}) = 2 * \Phi \left[ \sqrt{2} \left( -4 - 3 \sum_{i=1}^3 (4x_i - 2) \right) \right] - 1$$

where  $\Phi$  is the standard Gaussian CDF. We use  $d = 4$  and set the failure threshold at  $t = 0$ . We define the input distribution as  $x_i \stackrel{\text{ind}}{\sim} \mathcal{N}(0.6, 0.11)$  for  $i = 1, \dots, 4$ , truncated to  $[0, 1]$ .

## B Batch size comparison

Here we consider variations of the batch sizes used within the second stage of our design. When Stage 1 is complete and  $n$ -many evaluations have been spent on contour location, the remaining budget ( $B = N - n$ ) is to be spent on the highest entropy samples from  $X_M$ . Since the surrogate is used to select these samples, there is an option to select them in smaller batches, updating the surrogate with the new observations between each batch (indicated by the dotted arrow in Figure 1). But smaller batches require more computation as surrogate predictions must be obtained at all  $X_M$  locations after every batch update.

To investigate, we consider three different batch sizes for the Herbie function example of Section 4. First, we choose all high entropy points in a single batch of size  $B$  (this is the method used throughout the paper, thus these results are duplicated from Figure 6). Second, we consider selecting one high entropy point at a time, updating the surrogate after every high entropy point is observed to better inform the selection of subsequent high entropy points. Third, we consider selecting high entropy points in batches of size 10. Note, changing the batch size used within Stage 2 has no effect on Stage 1; each of these batch variations starts in the same place after the completion of contour location and uses the same  $X_M$ .

Figure 8 shows the resulting failure probability estimates across 30 Monte Carlo repetitions. There is no significant difference in performance among the three batch sizes. The grey shaded region marks  $\{\alpha \pm 2\sigma_\alpha\}$ ; it indicates the level of variability that we would expect from any Monte Carlo estimator of specified  $M$ , even if every sample was classified accurately. All methods consistently fall within this region, indicating effective estimation (note the narrower y-axis range compared to Figure 6). Given the computational expense of repeatedly updating the surrogate, we embrace the single batch approach.

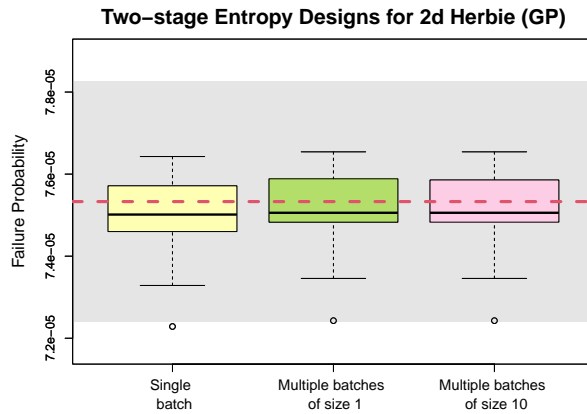


Figure 8: Estimated failure probabilities shown over the true failure probability (dashed red)  $\pm 2$  standard errors (grey shading) for proposed two-stage designs of the Herbie function. Variations use different batch sizes for selecting the highest entropy samples within Stage 2.